ce/papers Proceedings in civil engineering

Ernst & Sohn A Wiley Brand

ORIGINAL ARTICLE

eurosteel AMSTERDAM 2023

Ernst & Sohn A Wiley Brand

Insights into the occurrence of transverse bending stresses in web plates of crane runway girders

Paul Zauchner[1] | Markus Kettler[1] | Harald Unterweger[1]

Correspondence

Dipl.-Ing. Paul Zauchner
Graz University of Technology
Institute of Steel Structures
Lessingstraße 25/3
8010 Graz
Email: p.zauchner@tugraz.at

[1] Graz University of Technology, Austria

Abstract

Crane runway girders are installed in industrial buildings to carry heavy loads from crane operation. The wheels of the bridge crane introduce concentrated forces in the crane runway girder via the rails. This leads to local vertical stresses in the web plates of the crane runway girders in addition to the global bending stresses. The local stresses at the top of the web usually become crucial for the fatigue design of the girder. The potential eccentricity of vertical wheel loads as well as additional horizontal forces from operation of the crane can lead to torsional rotations of the rail and the top flange and subsequently to transverse bending of the web plate of the crane runway girder. In the current design model of EN 1993-6, the rotation at the top of the web plate is described by assuming the rail and the top flange of the girder acting as a bar under torsion, supported continuously by the bending stiffness of the web. Within this paper the existing model for the rotations is improved and it is shown that these modifications lead to more accuracy in comparison with numerical finite element calculations. It is also shown that the current simplified procedure for calculating the resulting stresses in the web is not able to adequately describe the real stresses for all practical cases. It is found that the quality of the stress predictions can significantly be improved by considering the web as a simply supported plate with the previously identified rotations on its top edge.

Keywords

crane runway girder, local stresses, plate bending

1 Introduction

Crane runway girders carry the loads from crane operation which are introduced over the wheels of the bridge crane into the crane rail. Due to the concentrated load introduction, vertical stresses occur in the webs of the crane runway girders additionally to the global longitudinal bending stresses. Since welded I-Sections in heavy crane operation are mainly used, the local vertical stresses near the welded connection between web and top flange of the girder are often decisive for the fatigue design.

During crane operation the wheel loads are acting with a certain eccentricity to the crane rail, caused by transvers drift of the crane track. The eccentricity of the vertical wheel loads, as well as horizontal loads lead to an additional torsion moment acting on the rail.

Fig.1 shows the stress components in the web of the crane runway girder induced by eccentric wheel load. The eccentricity e is specified in EN 1993-6 [1] with an equivalent value over all crane operations of $e = k/4 \leq t_w/2$, where k is the width of the rails head. Within this paper only the pure transverse bending component σ_T is investigated.

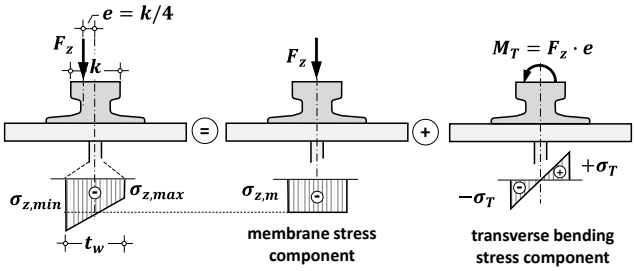

Figure 1 Stress components in the web plate of the crane runway girder due to eccentric wheel load

In the past, laboratory tests as well as numerical investigations have been carried out on this topic at Graz University of Technology [2], [3] and [4]. It was found that the transverse bending stresses in the web plate based on numerical finite element calculations can differ significantly from current code predictions. Furthermore, information on the accurate distribution of the transverse bending stresses in longitudinal direction of the web is missing. However, the distribution has an influence on the superposition of the stresses introduced by adjacent wheels. This is the motivation to investigate the occurrence of the

© 2023 The Authors. Published by Ernst & Sohn GmbH.

https://doi.org/10.1002/cepa.2526 wileyonlinelibrary.com/journal/cepa

This is an open access article under the terms of the Creative Commons Attribution-NonCommercial-NoDerivs License, which permits use and distribution in any medium, provided the original work is properly cited, the use is non-commercial and no modifications or adaptations are made.

transverse bending stresses in more detail and to find an improved calculation procedure.

1.1 Determination of transverse bending stresses according to current design standard

In EN 1993-6, the determination of the transverse bending stresses in the web plate is given by Eq. (1).

$$\sigma_T = \frac{6M_T}{a \cdot {t_w}^2} \cdot \eta \cdot tanh(\eta) \tag{1}$$

where: $\eta = \left[\frac{0.75\, a\, {t_w}^3}{I_t} \cdot \frac{sinh^2(\pi \cdot h_w/a)}{sinh(2\pi \cdot h_w/a) - 2\pi \cdot h_w/a}\right]^{0.5}$

These formulae are mainly based on works in [5] and [6]. It is assumed that the crane rail and the top flange of the crane girder act together as a torsion bar with fork end conditions at the location of the transverse stiffeners and by a certain rotational restraint of the web $\bar{c}_\varphi$ (see Fig. 2). The length of the investigated torsion bar corresponds to the distance a between adjacent transverse stiffeners.

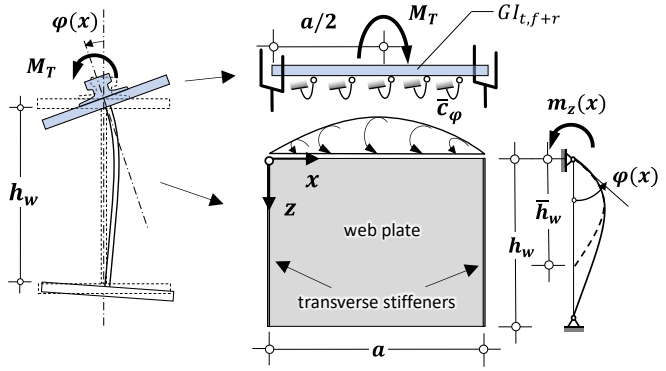

Figure 2 Analytic model for calculating the top flange rotation $\varphi(x)$ according to [5]

The introduction of the external torsion moment $M_T = F_z \cdot e$ which occurs due to eccentric position of the wheel load F_z leads to a torsional rotation $\varphi(x = a/2)$ of the crane rail and the top flange. In terms of compatibility, this torsional rotation φ is forced to the web plate which leads to transverse bending of the web. The determination of the rotational restraint $\bar{c}_\varphi$ is recommended in [6] with Eq. (2),

$$\bar{c}_\varphi = \frac{3E{t_w}^3}{12 \cdot \bar{h}_w(1-\nu^2)} \tag{2}$$

where the reduced web height of the plate $\bar{h}_w$ can be determined by means of Eq. (3).

$$\bar{h}_w = \frac{3a}{4\pi} \cdot \frac{sinh\left(\frac{2\pi}{a}h_w\right) - \frac{2\pi}{a}h_w}{sinh^2\left(\frac{\pi}{a}h_w\right)} \tag{3}$$

The transverse bending stresses on the top edge of the web plate are calculated by multiplying the plate edge moment $m_z(x, z = 0)$ with the flexural bending resistance of a plate strip, see Eq. (4). The plate edge moment $m_z(x, z = 0)$ on the top edge of the web is calculated by multiplying the maximum value of the rotation φ, for load introduction at $x = a/2$, with the constant rotational stiffness $\bar{c}_\varphi$ of the web according to Eq. (2).

$$\sigma_T = m_z \cdot \frac{6}{{t_w}^2} = \varphi \cdot \bar{c}_\varphi \cdot \frac{6}{{t_w}^2} \tag{4}$$

The determination of the bending stresses with Eq. (4) is equivalent to Eq. (1). It considers the web plate only acting as a plate strip. It neglects the real behavior of the web acting as a plate which is supported by the flanges on its top and bottom edges and by the transverse stiffeners on its lateral edges.

2 Proposal for the determination of transverse bending stresses

Numerical investigations identified that the real transverse bending stresses of the web plate can only be roughly approximated with the current design model, because the web plate is only considered with its constant stiffness $\bar{c}_\varphi$. It can be shown within this paper, that the quality of the stress predictions can significantly be improved by considering plate bending effects by means of classic plate theory. However, for an accurate description of the behavior it is also necessary to get a more accurate analytical solution for the top flange torsional rotations.

For determining the rotations of the top flange, it is proposed to use the torsion bar model from [5] and to additionally consider the warping stiffness of the rail only (see Fig. 3).

Once the rotations of the top flange are determined (see section 2.1), the plate edge moments and the transverse bending stresses of the web plate can be determined with an analytic plate model (see section 2.2).

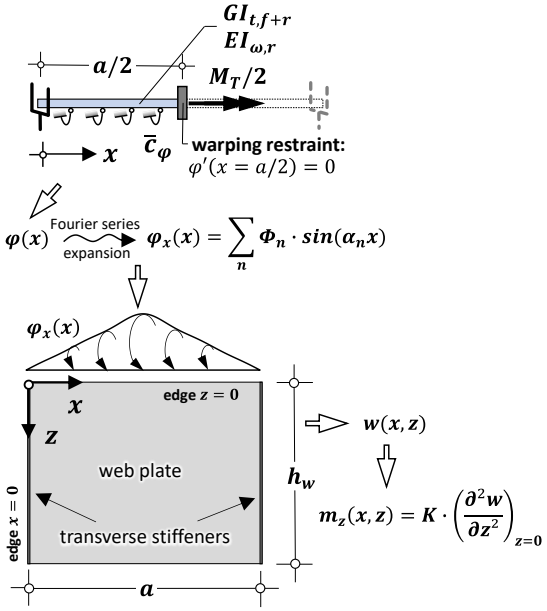

Figure 3 Overview of the procedure to calculate the transverse bending stresses in the web plate

2.1 Modified analytical solution for the rotations of the top flange

The model for determining the torsional rotation according to [5] (see Fig. 2) is extended by the warping stiffness of the rail, see Fig. 3. Due to the single point load introduction of the external torsion moment, there is a kink in the distribution of the rotation $\varphi(x)$ proposed in [5]. In real crane girders there is no single point load introduction possible, but limited load distribution caused by the rail. Forcing a horizontal tangent to the distribution of rotation

25097075, 2023, 3-4, Downloaded from https://onlinelibrary.wiley.com/doi/10.1002/cepa.2526 by CochraneAustria, Wiley Online Library on [17/11/2023]. See the Terms and Conditions (https://onlinelibrary.wiley.com/terms-and-conditions) on Wiley Online Library for rules of use; OA articles are governed by the applicable Creative Commons License

would lead to more accurate results. This was realized by also considering the warping stiffness of the rail.

The high warping stiffness of the rail leads to a full warping restraint in the symmetry plane for load introduction at the half span between two transverse stiffeners, $x = a/2$ (see Fig. 3). Subsequently the warping restraint leads to a horizontal tangent in the distribution of the rotation $\varphi(x)$.

The modified bar under torsion, shown in Fig. 3 can be described with the differential equation in Eq. (5).

$$EI_{\omega,r}\varphi^{IV} - GI_t\varphi^{II} + \bar{c}_\varphi\varphi = 0 \quad (5)$$

In Eq. (5) $I_{\omega,r}$ is the warping constant of the rail related to the assumed rotation axis at the bottom of the rail. I_t is the common torsion constant of the rail and the top flange of the girder and $\bar{c}_\varphi$ is the rotational restraint of the web according to [6] (see Eq. (2)).

Introducing the factors $\alpha = GI_t/2EI_{\omega,r}$ and $\beta = \bar{c}_\varphi/EI_{\omega,r}$ leads to the form of the differential equation according to Eq. (6):

$$\varphi^{IV} - 2\alpha\varphi^{II} + \beta\varphi = 0 \quad (6)$$

With $\varphi(x) = C \cdot e^{\lambda x}$ the homogeneous form of the differential equation can be written as shown in Eq. (7):

$$\varphi(x) = C_1 \cdot e^{\lambda_1 x} + C_2 \cdot e^{-\lambda_1 x} + C_3 \cdot e^{\lambda_2 x} + C_4 \cdot e^{-\lambda_2 x} \quad (7)$$

where: $\lambda_1 = \sqrt{\alpha + \sqrt{\alpha^2 - \beta}}$ and: $\lambda_2 = \sqrt{\alpha - \sqrt{\alpha^2 - \beta}}$

with: $\alpha^2 \geq \beta$

For solving the constants C_1 to C_4 the following four boundary conditions are utilized:

For $x = 0$:

$$\varphi(x = 0) = 0 \quad (8a)$$

$$-EI_{\omega,r} \cdot \varphi''(0) = 0 \quad (8b)$$

and for $x = a/2$:

$$-EI_{\omega,r} \cdot \varphi'''(a/2) + GI_t \cdot \varphi'(a/2) = M_T/2 \quad (8c)$$

$$\varphi'(x = a/2) = 0 \quad (8d)$$

The boundary condition in Eq. (8b) is a simplification. The ongoing rail over the transverse stiffener would act like a warping spring. But it can be shown that these effects are neglectable for the case with maximum bending stresses at the load introduction. Solving the equation system with the four boundary conditions leads to the following analytic solution for the rotations of the crane girders top flange:

$$\varphi(x) = \frac{M_T}{2EI_{\omega,r}(\lambda_2{}^2 - \lambda_1{}^2)} \cdot \left(\frac{sinh(\lambda_1 x)}{\lambda_1 cosh\left(\lambda_1 \frac{a}{2}\right)} - \frac{sinh(\lambda_2 x)}{\lambda_2 cosh\left(\lambda_2 \frac{a}{2}\right)} \right); \; 0 \leq x \leq \frac{a}{2} \quad (9)$$

It is noted, that $\varphi(x)$ in Eq. (9) is symmetric regarding to the symmetry plane of the web plate at $x = a/2$.

2.2 Determination of the transverse bending stresses in the web plate

The transverse bending of the web plate occurs based on compatibility. The top edge of the web plate has the same rotation $\varphi(x)$ as the top flange of the girder. Considering the web acting as a plate means that the homogeneous solution of the differential equation for a rectangular plate with hinged supports on all four edges is needed. In [7] the homogeneous solution can be found as:

$$w(x,z) = \frac{sin(\alpha_n x)}{\alpha_n{}^2}\left(A_1 \cdot cosh(\alpha_n z) + \alpha_n z A_2\, sinh(\alpha_n z) + A_3\, sinh(\alpha_n z) + \alpha_n z A_4 cosh\,(\alpha_n z)\right) \quad (10)$$

On the top edge of the plate (edge z=0 in Fig. 3) the boundary condition of the plate is defined by the previously identified rotation $\varphi(x)$ of the top flange according to Eq. (9). This was realized by means of the following Fourier series expansion ($\varphi(x)$ is assumed to be $2a$ periodic):

$$\varphi_x(x) = \sum \Phi_n sin\,(\alpha_n x); \quad (11)$$

where $\alpha_n = \frac{n\pi}{a}$ and $\Phi_n = \frac{2}{a} \cdot \int_0^a \varphi(x) \cdot \sin\,(\alpha_n x)dx =$

$$= \frac{2M_T a}{EI_{\omega,r}(\lambda_2{}^2 - \lambda_1{}^2)} \cdot \left[\frac{sin(n\pi/2)}{a^2\lambda_1{}^2 + n^2\pi^2} - \frac{sin(n\pi/2)}{a^2\lambda_2{}^2 + n^2\pi^2}\right]$$

In Eq. (11), Φ_n is only none-zero if $n = 1, 3, 5\ldots$.

Now the following boundary conditions can be formed for solving the constants A_1 to A_4 in Eq. (10):

$$w(x, z = 0) = 0 \quad (12a)$$

$$w(x, z = h_w) = 0 \quad (12b)$$

$$\left(\frac{\partial w}{\partial z}\right)_{(x,\ z=0)} = \varphi_x(x) \quad (12c)$$

$$\left(\frac{\partial^2 w}{\partial z^2}\right)_{(x,\ z=h_w)} = 0 \quad (12d)$$

Inserting the terms of Eq. (12a) to Eq. (12d) in Eq. (10) and considering its derivatives leads to the following form which represents the deformation of the web plate due to the predefined rotation $\varphi_x(x)$ on the top edge:

$$w(x,z) = \frac{\Phi_n}{f_{zn}} \cdot sin\,(\alpha_n x) \cdot \left[\left(h_w \cdot \left(1 - coth^2(\alpha_n h_w)\right) - z\right) \cdot sinh(\alpha_n z) + z \cdot coth\,(\alpha_n \cdot h_w) \cdot cosh\,(\alpha_n z)\right] \quad (13)$$

where $f_{zn} = coth(\alpha_n \cdot h_w)\,(1 - \alpha_n \cdot h_w \cdot coth(\alpha_n \cdot h_w)) + \alpha_n \cdot h_w$

Once the deformation shape $w(x,z)$ is known, the resulting edge moment of the web plate can be calculated:

$$m_z(x, z = 0) = -K \cdot \left(\frac{\partial^2 w}{\partial z^2} + \nu\frac{\partial^2 w}{\partial x^2}\right)_{z=0} = 2K \cdot \sum \frac{\Phi_n \alpha_n}{f_{zn}} sin\,(\alpha_n x) \quad (14)$$

where K is the plate bending stiffness of the web $K = \frac{Et_w{}^3}{12(1-\nu^2)}$. The term $\nu\frac{\partial^2 w}{\partial x^2}$ gets zero, since no out of plane deformation can occur on the top edge $z = 0$, due to the support.

Finally, the bending stresses on the top edge of the web plate can be calculated by multiplying the edge moment with the flexural bending resistant of the web plate.

25097075, 2023, 3-4, Downloaded from https://onlinelibrary.wiley.com/doi/10.1002/cepa.2526 by CochraneAustria, Wiley Online Library on [17/11/2023]. See the Terms and Conditions (https://onlinelibrary.wiley.com/terms-and-conditions) on Wiley Online Library for rules of use; OA articles are governed by the applicable Creative Commons License

$$\sigma_T = m_z(x, z=0) \cdot \frac{6}{{t_w}^2} = \frac{E \cdot t_w}{(1-\nu^2)} \cdot \sum \frac{\Phi_n \alpha_n}{f_{zn}} sin\,(\alpha_n x) \qquad (15)$$

3 Finite element parametric study and comparison with the analytical model

To investigate the accuracy of the proposed calculation procedure, a numerical parametric study was carried out. 24 crane runway girders with different cross section configurations were investigated. For the parametric study within this paper a crane rail A 100 (k =100) without elastomeric bearing pad was considered for all cross sections. Two different distances a of the transverse stiffeners were investigated depending on the web height ($a/h_w = 1.0$ and $a/h_w = 2.0$). The investigated cross sections are summarized in Table 1.

3.1 Elastic finite element analysis

The elastic finite element calculations were performed with the software Abaqus. Since only the local vertical stresses were investigated, only a local model consisting of a part of a crane runway girder with the length $L = 3a$ was modelled, including the transverse stiffeners. Therefore, global bending effects are negligible, but the influence of the adjacent web fields is considered. The rail and the crane runway girder are modelled with 3D solid elements from the type C3D8R. The web of the crane runway girders was modelled with elements with a quadratic basis function (type C3D20R). The transverse stiffeners are modelled as shells with a thickness of t_s = 10 mm for all cross sections. The contact between the rail and the girder was formulated for a rail bedded on the top flange without any interlayer as a hard contact with separation allowed. The outer edges of the rails foot were continuously fixed to the top flange to prevent the rail from uplift during rotation due to the external torsion moment. On real crane girders, rail is fixed in discrete distances by the rail clamps.

The introduction of the eccentric wheel load was realized by a combination of a concentric vertical force F_z = 500 kN and an additional torsion moment resulting from an eccentricity of the load from a quarter of the rails head width, $M_T = F_z \cdot k/4 = 500 \cdot 0.025 = 12.5$ kNm. Since the load introduction is in the half span between two transverse stiffeners, symmetry conditions are utilized.

Fig. 4 shows the result paths in the finite element model on both sides of the web plate near the top flange where the vertical displacements u_z and the vertical stresses σ_z are evaluated.

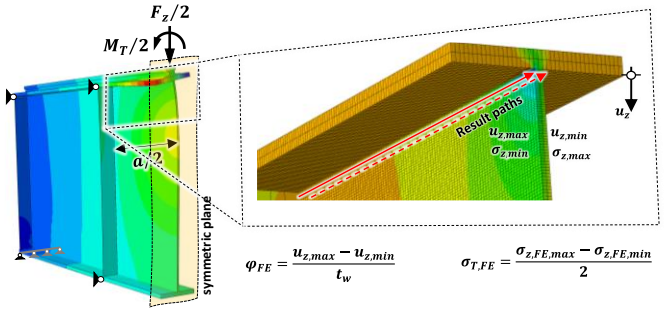

Figure 4 3D – Finite element model and used result paths for determining the torsional rotations φ_{FE} and transverse bending stresses $\sigma_{T,FE}$

The cross-sectional parameters of the used profile rail A 100 are summarized in Table 2. For the rail A 100 an abrasion of 12.5% of the rail heads height was assumed. The cross-sectional parameters for a rail with abrasion $h_{r,12.5\%}$ and $I_{t,r}$ were adopted from [8]. The rotation axis for the calculation of $I_{\omega,r}$ was assumed in the intersection of the symmetry axis at the bottom of the rail.

The rotations φ_{FE} are calculated based on the vertical displacements $u_{z,i}$ and the transverse bending stresses $\sigma_{T,FE}$ are based on the vertical stresses $\sigma_{z,i}$ from the 3D FE-calculation according to the equations in Fig. 4.

Table 1 cross section dimension of the investigated crane girders

Cross section	t_w [mm]	h_w [mm]	t_f [mm]	b_f [mm]	$\bar{h}_w$ [mm]	$\bar{c}_\varphi$ [N]
CS 1	10	2000	20	400	936.0	61636
CS 2	13	2000	20	400	936.0	135415
CS 3	15	2000	20	400	936.0	208023
CS 4	18	2000	20	400	936.0	359464
CS 5	20	2000	20	400	936.0	493092
CS 6	15	2000	25	400	936.0	208023
CS 7	15	2000	30	400	936.0	208023
CS 8	15	2000	35	400	936.0	208023
CS 9	15	2000	40	400	936.0	208023
CS 10	10	2000	40	400	936.0	61636
CS 11	20	2000	40	400	936.0	493092
CS 12	15	2000	45	400	936.0	208023
CS 13	15	2000	30	300	936.0	208023
CS 14	15	2000	30	220	936.0	208023
CS 15	15	2000	30	800	936.0	208023
CS 16	10	1000	20	400	468.0	123273
CS 17	15	1000	20	400	468.0	416046
CS 18	20	1000	20	400	468.0	986183
CS 19	15	1000	30	400	468.0	416046
CS 20	15	1000	40	400	468.0	416046
CS 21	15	1000	45	400	468.0	416046
CS 22	15	1000	30	220	468.0	416046
CS 23	15	1000	30	300	468.0	416046
CS 24	15	1000	30	800	468.0	416046

Table 2 cross-sectional parameters of the profile rail A100

Crane rail	k [mm]	$h_{r,12.5\%}$ [mm]	$I_{t,r}$ [cm⁴]	$I_{\omega,r}$ [cm⁶]
A100	100	90	580.6	10078.7

3.2 Comparison of FE-analysis with the new proposal

Fig. 6 shows the comparison of the torsional rotations $\varphi(x)$ on the top edge of the web from the FE-analyses with the analytical solution in [5] and with the modified analytical solution according to Eq. (9) exemplarily for four selected cross sections. The distributions of torsional rotations are plotted for over the nondimensional coordinate x/a, so two different aspect ratios of the web can be shown for each selected cross section (a/h_w = 1.0; 2.0). Since the results

25097075, 2023, 3-4, Downloaded from https://onlinelibrary.wiley.com/doi/10.1002/cepa.2526 by CochraneAustria, Wiley Online Library on [17/11/2023]. See the Terms and Conditions (https://onlinelibrary.wiley.com/terms-and-conditions) on Wiley Online Library for rules of use; OA articles are governed by the applicable Creative Commons License

are symmetric for load introduction at half span between the transverse stiffeners, the results are plotted for the central web field from the position of the transverse stiffener $x/a = 0$ to the position of load introduction at $x/a = 0.5$. The dimensions of the selected cross sections CS3, CS9, CS17 and CS 20 are given in Table 1. CS3 and CS9 have a web height of 2000 mm, while CS17 and CS 20 have a web height of 1000 mm. Cross sections CS 9 and CS 20 have thicker flanges (t_f = 40 mm) than cross sections CS 3 and CS 17 (t_f = 20 mm). The distributions of the torsional rotations $\varphi(x)$ in Fig. 5 show that the shape of the FE-analysis fits very well with the new modified analytical model but also with the model according to [5]. Near the load introduction at $x/a = 0.5$ it can be verified that the proposed additional consideration of the warping stiffness of the rail can describe the results from the FEA in a more accurate way for all cases. In Fig. 6 the transverse bending stresses determined with FE-analysis are compared with the maximum value calculated with the formulae in EN 1993-6 (EC 3-6, see Eq. (1)) and the results based on plate theory according to Eq. (15), with the rotation $\varphi(x)$ of the modified analytical model. The comparison in Fig. 6 is carried out for the same selected cross sections. The comparison in Fig. 6 shows, that the determination of the transverse bending stresses via plate theory can describe the distribution of the FE-results quite well in contrast to EN 1993-6 (EC 3-6). It can be identified that the significant local increase of the bending stresses near the half span of the plate can adequately be described only with the plate theory.

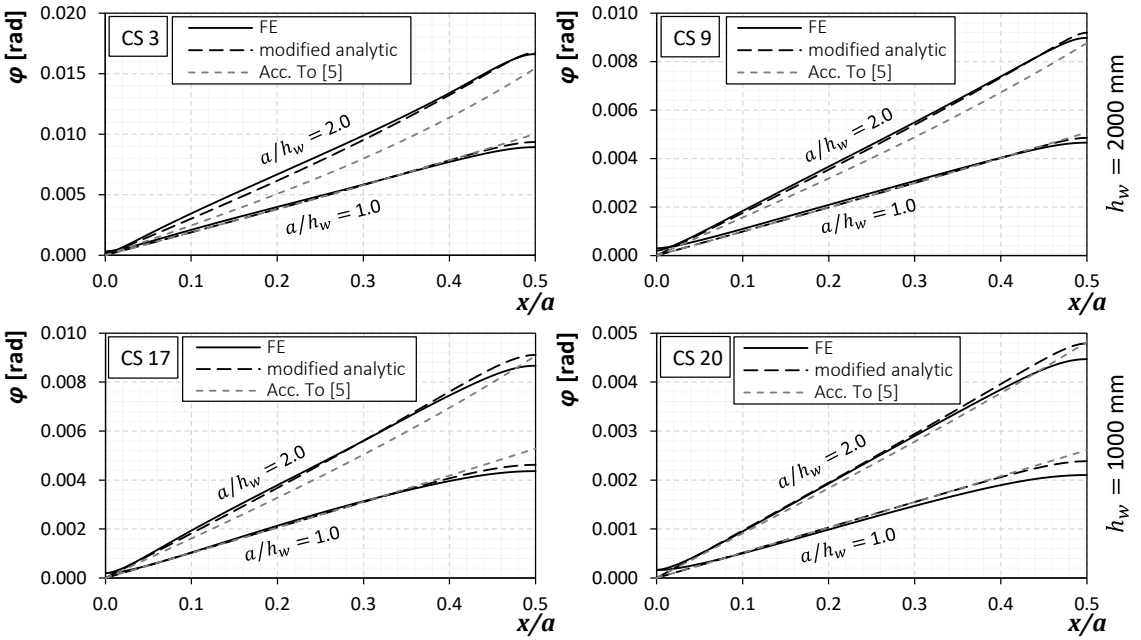

Figure 5 Comparison of the torsional rotations $\varphi(x)$ calculated with the modified analytical model, according to [5] and based on FE-analysis

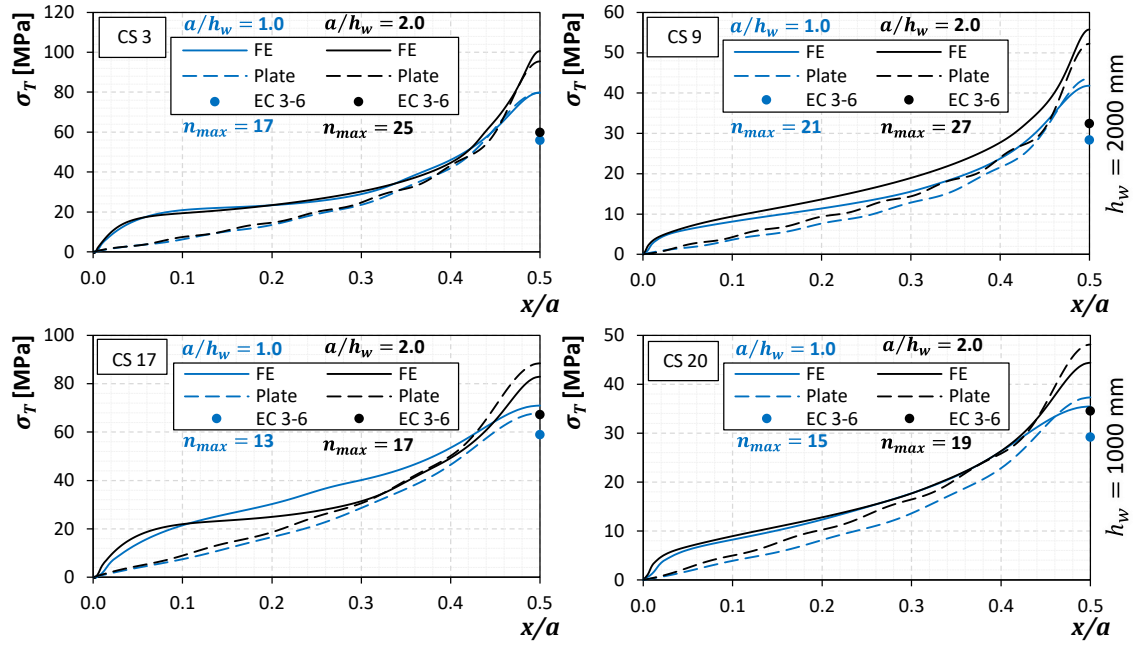

Figure 6 Comparison of transverse bending stresses $\sigma_T(x)$ determined from the proposed plate model (Plate), the maximum value calculated with EN 1993-6 [1] (EC 3-6) and determined based on FE-analysis (FE)

25097075, 2023, 3-4, Downloaded from https://onlinelibrary.wiley.com/doi/10.1002/cepa.2526 by CochraneAustria, Wiley Online Library on [17/11/2023]. See the Terms and Conditions (https://onlinelibrary.wiley.com/terms-and-conditions) on Wiley Online Library for rules of use; OA articles are governed by the applicable Creative Commons License

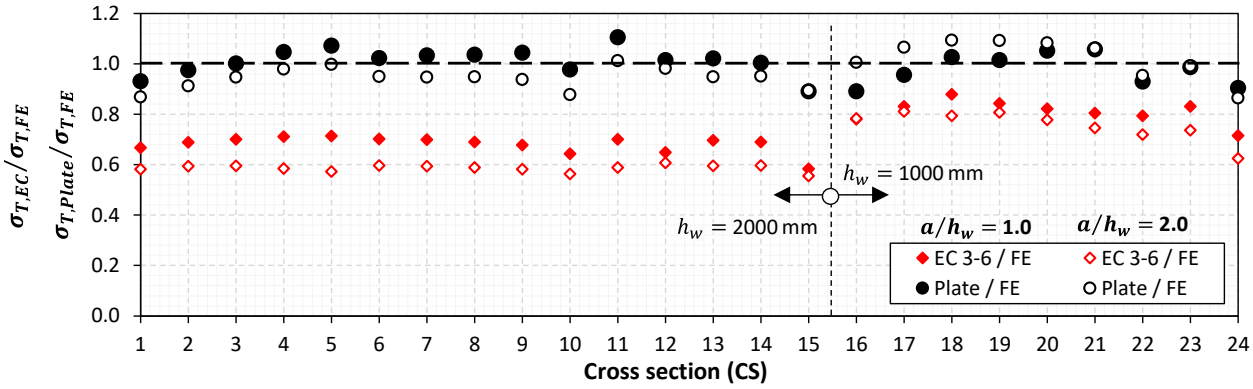

Figure 7 Comparison of the related maximum bending stresses $\sigma_{T,Plate}/\sigma_{T,FE}$ and $\sigma_{T,EC}/\sigma_{T,FE}$ for all investigated crane girder cross sections

This local stress increasing effect is completely neglected with the determination according to EN 1993-6 [1] since a constant stiffness of the web is assumed which results in an underestimation of the maximum bending stresses. The highest recommended number of Fourier series terms n_{max} which is used for Eq. (14) depends on the total length of the plate a. This is due to the fact, that the domain of locally increased bending stresses gets smaller with higher lengths a. So higher numbers n_{max} are needed to cover this area. A termination criterion was used if the increase of the maximum stress value is lower than 1% compared to the preceding sum term. It is evident from Fig. 6 that the distributions differ near the transverse stiffener. This can be explained with clamping effects in the FEA, since the transverse stiffener is connected rigidly to the web and the top flange while the plate stress equations are determined for a hinged edge of the plate. However, it is pointed out, that it is possible to consider the clamping effects using the plate equations, but it is not carved out within this paper.

Fig. 7 shows the maximum values for the bending stresses referred to the FE-results determined with the proposed solution based on plate theory ($\sigma_{T,Plate}/\sigma_{T,FE}$) and determined according to EN 1993-6 ($\sigma_{T,EC}/\sigma_{T,FE}$) for the 24 investigated crane runway girder cross sections (see Table 1). It can be shown, that these values determined with plate theory have a bandwidth from $\sigma_{T,Plate}/\sigma_{T,FE}$ = 0.86 to 1.11 (mean value = 0.99) while the determination with the code underestimates the maximum bending stresses across all cross sections with $\sigma_{T,EC}/\sigma_{T,FE}$ = 0.55 to 0.88 (mean value = 0.69).

4 Conclusions

Within this paper it is illustrated that the quality of the prediction of local transverse bending stresses in the web plate of a crane runway girder can be enhanced significantly with the following two improvements:

(i) Consideration of the warping stiffness of the rail: This modification of the torsion bar model in [5] leads to a more accurate prediction for the rotation $\varphi(x)$ in comparison with FE results. The forced horizontal tangent in the symmetry plane at the wheel load also causes a faster convergence in the Fourier series expansion (smaller number n needed).

(ii) Determining the transverse bending stresses in the web plate via plate theory: This paper illustrates that a consideration of the web acting as a plate is necessary to predict an accurate distribution of the transverse bending stresses in longitudinal direction. Local increasing of the bending stresses near the wheel load at the half span between the transverse stiffeners is also considered with this new proposed procedure.

The determination of bending stresses with a constant stiffness of the web in longitudinal direction in [1] leads to a significantly underestimation of the maximum bending stresses. Finally, the authors would like to point out that the in some cases drastic underestimation of the bending stresses by EN 1993-6 is put into perspective by the fact that the bending stress component represents only 30% to 40% of the total vertical stresses σ_z.

References

[1] EN 1993-6: Eurocode 3: *Design of steel structures – Part 6: Crane supporting structures,* CEN, Brussels, 2007

[2] M. Kettler, A. Kampleitner, F. Novak, A. Mandl, H. Unterweger: *Local stresses in webs of crane runway girders: Tests and numerical calculations,* J. Constr. Steel Res. 2017; 139: 188-201

[3] M. Kettler, C. Derler, A. Schörghofer, C. Macho, H. Unterweger: *Laboratory tests on real crane runway girder with box section,* J. Constr. Steel Res. 2019; 160: 540-58

[4] M. Kettler, F. Kiem, H. Unterweger: *Local stresses in retrofitted crane runway girders with boxed upper flange due to eccentric wheel loading,* Structures, 2020; 25: 646-659

[5] J. Oxfort: *Zur Beanspruchung der Obergurte vollwandiger Kranbahnträger durch Torsionsmomente und durch Querkraftbiegung unter dem örtlichen Radlastangriff,* Der Stahlbau 32 (1963) 360–367

[6] J. Oxfort*: Zur Biegebeanspruchung des Stegblechanschlusses infolge exzentrischer Radlasten auf dem Obergurt von Kranbahnträgern,* Der Stahlbau 50 (1981) 215–217

[7] K. Girkmann*: Flächentragwerke,* 5th improved and increased edition Vienna, Springer; 1959

[8] M. Kraus, S. Mämpel: *Kennwerte neuer und abgenutzter Schienen für die Bemesung von Kranbahnträgern,* Stahlbau 2017; 86:36-44

25097075, 2023, 3-4, Downloaded from https://onlinelibrary.wiley.com/doi/10.1002/cepa.2526 by CochraneAustria, Wiley Online Library on [17/11/2023]. See the Terms and Conditions (https://onlinelibrary.wiley.com/terms-and-conditions) on Wiley Online Library for rules of use; OA articles are governed by the applicable Creative Commons License